Molecular structure and chiral separation in α-sexithiophene ultrathin films on Au(111): Low-energy electron diffraction and scanning tunneling microscopy

Mario Kiel, Klaus Duncker, Christian Hagendorf, and Wolf Widdra
Institute of Physics, Martin-Luther-Universität Halle-Wittenberg, Halle, Germany
(Received 24 February 2007; published 29 May 2007)

The adsorption of the π-conjugated organic molecule α-sexithiophene which is widely used in molecular electronics has been studied on Au(111) by low-energy electron diffraction and scanning tunneling microscopy. For monolayer adsorption at room temperature, large, well-ordered domains of flat-lying molecules which arrange in molecular rows are observed. A detailed structure analysis reveals an incommensurate, line-on-line oriented monolayer with one molecule per unit cell. In contrast to the behavior in the three-dimensional bulk structure, flat-lying adsorption introduces molecular chirality: Right- and left-handed molecules separate into domains of different orientations which are mirror symmetric with respect to the $[11\bar{2}]$ substrate direction. Details of the adlayer structure and the chiral self-recognition can be rationalized based on the van der Waals contour of the adsorbed molecules.

DOI: 10.1103/PhysRevB.75.195439 PACS number(s): 68.55.−a, 68.43.Fg, 61.14.Hg, 68.37.Ef

I. INTRODUCTION

In the wide field of molecular electronics, the nanoscopic and mesoscopic order in thin films of π-conjugated organic molecules are of great importance for the performance in low-cost electronic and optoelectronic devices as solar cells, light-emitting diodes, and field-effect transistors. This has driven many investigations of adsorption and growth of thin films on various substrates as reviewed recently.[1–3] One promising class of larger π-conjugated organic molecules is based on oligothiophenes and their derivates. The physical properties of oligothiophenes can be tuned by the number of thiophene rings or by functional groups. Often oligothiophenes serve as a model system for the structural less controllable polythiophene. In the bulk crystal, α-sexithiophene (6T) adopts a herringbone structure with two and four planar molecules in a high-temperature and a low-temperature monoclinic phase, respectively.[4,5] In both structures the two different species of planar molecules are inclined with respect to the other.[4]

For adsorption on close-packed metal surfaces and on highly oriented graphite (HOPG) monolayer structures of 6T and of the related α-quarterthiophene (4T) with their molecular planes parallel to the surface have been reported. Especially the adsorption of 4T, 6T, and end-capped forms of these molecules have been studied on various noble metal surfaces.[1,3,6–20] On Cu(111), adsorption with the molecular plane parallel to the surface has been found for the initial growth[21] which continues for growth temperature of 360 K and higher coverages with a perpendicular molecular orientation as found also for many other substrates.[3] More detailed structural information on the oligothiophene monolayer unit cell has been determined on Ag(111) for 4T, end-capped 4T, end-capped 6T.[1,6,10,13] For 6T adsorption on Ag(110) and on Ag(111), a flat and commensurate adsorption with the molecular axis aligned in the high-symmetry [001] and $[1\bar{1}0]$ directions, respectively, has been proposed based on NEXAFS and RHEED results.[16] On Au(111), there is to our knowledge no structural information available. Only on a strongly vicinal Au(111) surface 6T adsorption has been studied so far.[17] On Au(111) the adsorption of hexaphenyl (6P) molecules which are π-conjugated molecules of comparable size have been investigated recently.[22] However, due to the absence of sulfur in these molecules their symmetry and, most likely, their bonding to the substrate are different from 6T.

Despite the numerous studies on 6T thin films and their promising optical as well as electronic properties, there is a lack of knowledge on the *detailed* molecular structure of the first monolayer which must serve as a template for any further growth. Therefore, we present here a combined high-resolution scanning tunneling microscopy (STM) and low-energy electron diffraction (LEED) study on the initial state of adsorption. It will be shown that the monolayer structure consists of highly ordered homochiral domains of flat-lying molecules with all-*trans* conformation of the thiophene rings. Many aspects of the molecular structure will be traced back to an optimization of a dense monolayer structure accounting for the van der Waals contour of the flat-lying molecule shown in Fig. 1(c).

On flat metal substrates 6T adsorption is possible with two different adsorbed species as illustrated in Figs. 1(a) and

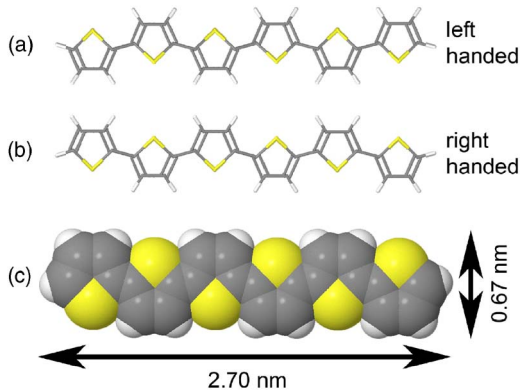

FIG. 1. (Color online) Sketch of the α-sexithiophene (6T) molecule. Note the two possible chiralities upon adsorption on a flat metal surface shown in (a) and (b). The van der Waals dimensions of the molecules are depicted in (c).

1(b). Both species have opposite chirality depending on the orientation of their sulfur groups. This is a specific property of oligothiophenes with an *even* number of thiophene rings which have a C_2 symmetry axis along the surface normal. On the other hand, oligothiophenes with an *odd* number of rings exhibit C_S symmetry and are nonchiral. Assuming that surface diffusion occurs as a flat-lying molecule by largely maintaining the attractive molecule-substrate interaction, the chirality of the adsorbed molecules is fixed during diffusion and monolayer growth. The influence of molecular chirality for oligothiophene thin-film growth will be experimentally demonstrated here; a thin-film concept which is absent in the three-dimensional (3D) bulk structure. Chirality at surfaces has been discussed largely in the context of heterogeneous enantioselective catalysts with applications in the chemical and pharmaceutical industries (see, e.g., Ref. 23). But additionally the optical properties are expected to be different for domains of opposite chirality and to lead, e.g., to circular dichroism.[24]

II. EXPERIMENTAL DETAILS

The measurements were performed in a two-chamber UHV system with a base pressure of about 10^{-10} mbar. The analysis chamber is equipped with diagnostics for XPS (CSA300, Omicron Nanotechnology), LEED, SEM, and room-temperature AFM/STM (Omicron Nanotechnology). For the STM measurements tips etched from 0.2 mm tungsten wire were used. For calibration of the STM piezoelements, imaging of Si(100)-(2×1) and Au(111) samples with atomic resolution was used. The preparation chamber is equipped with Ar^+ ion sputtering and heating facilities as well as a homebuilt Knudsen cell operating at about 500 K for sublimation of the 6T molecules. The Au(111) surface was prepared by cycles of subsequent Ar^+ ion sputtering and annealing to 620 K. Sample cleanliness and long-range order was verified by XPS, LEED, and STM.

Thin films of 6T molecules, purchased from Syncom, were sublimated without further cleaning processes. Typical growth rates for adsorption on the Au(111) of 0.2 monolayer (ML) per minute were used with the sample at room temperature.

III. RESULTS

STM images of the bare and the α-sexithiophene (6T) covered Au(111) surfaces are shown in Fig. 2. The STM image of the clean Au(111) surface, Fig. 2(a), exhibits the well-known herringbone reconstruction on two different (111) terraces which consists of stripes running dominantly along the three equivalent $[11\bar{2}]$ high symmetry directions. Figure 2(b) displays the bare surface on an enlarged scale which allows for atomic resolution of the $(22\times\sqrt{3})$ reconstruction.[25–28] The two vertical areas which appear lighter in Fig. 2(b) correspond to surface Au atoms occupying bridge sites and can be distinguished from darker fcc and hcp regions.

Upon 6T adsorption at room temperature, large scale STM images as shown in Fig. 2(c) demonstrate that the herringbone reconstruction is still present and is superimposed on the monolayer structure of the 6T molecular film. The region marked by a black square in Fig. 2(c) is enlarged in Fig. 2(d). Well-ordered rows of 6T molecules can be identified in Fig. 2(d). These rows are oriented along a direction characterized by a small but finite angle with respect to the $[11\bar{2}]$ high symmetry direction. The latter is visible in the STM images via the Au(111) herringbone reconstruction. At substrate steps, 6T molecules are found which are preferentially oriented parallel to the substrate step edges as seen in Fig. 2(c). High-resolution images, as in Fig. 2(e), show that individual molecules within large domains can be imaged as a rodlike structure with an internal corrugation with six maxima. We assign the internal structure to the six thiophene rings within each molecule. The molecules are oriented nearly perpendicular to the row direction. Adjacent rows are shifted with respect to each other in the row direction. This leads to a periodic structure with a nonrectangular unit cell with one molecule per unit cell as indicated in Fig. 2(e). Here, the long 6T molecular axis is rotated against the long unit cell axis and exactly perpendicular to the short unit cell axis.

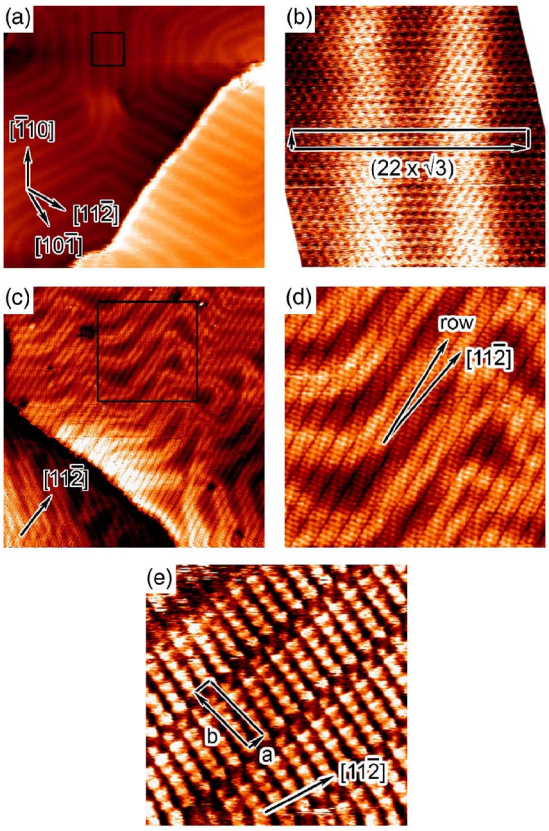

FIG. 2. (Color online) STM images of the Au(111) surface before and after adsorption of α-sexithiophene (6T) at room temperature: (a) Bare Au(111) (60×60 nm^2, –0.8 V, 1.0 nA); (b) enlarged region of (a) (6.5×6.5 nm^2); (c) monolayer of 6T adsorbed on Au(111) (100×100 nm^2, –1.5 V, 0.3 nA); (d) enlarged region of (c) (38×38 nm^2); (e) monolayer structure with submolecular resolution (10×10 nm^2, –0.18 V, 0.6 nA).

To analyze the internal 6T ring structure for molecules in adjacent rows, an averaged line profile across seven rows of

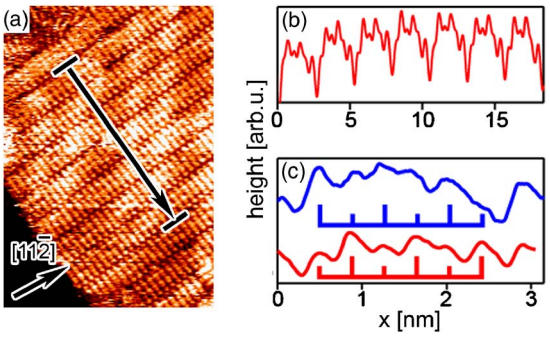

FIG. 3. (Color online) (a) STM image of one homochiral 6T domain on Au(111) (30×30 nm^2, −0.21 V, 0.3 nA). (b) Line profile across seven molecular rows as marked in (a) indicating alternating apparent heights of the thiophene subunits within each molecule. (c) Enlarged line profile along single molecules within the two different homochiral domains as marked in the inset of Fig. 4.

6T molecules is shown in Fig. 3(b). The profile corresponds to the line sketched in Fig. 3(a). The line profile shows a distinct structure which is repeated periodically. The period of about 2.6 nm corresponds to the width of a single molecular row and approximately to the length of the 6T molecule. Its internal structure [see also Fig. 3(c)] exhibits six equidistant features of alternating apparent height. We assign these features to the thiophene rings with alternating sulfur orientation. The identical sequence of sulfur orientations in all molecules along the line profile in Fig. 3(b) is a clear evidence for the presence of a homochiral domain in Fig. 3(a): identical orientation and chirality of molecules within rows and in adjacent rows. The lower trace in Fig. 3(c) shows a similar line scan (see below) on an enlarged scale. The positions of the alternately oriented thiophene rings within one molecule are marked by bars. Figure 4 displays an STM image of the 6T monolayer on a large terrace where two nonequivalent domains are visible. It was prepared and imaged under similar conditions as in Figs. 2(c)–2(e). The boundary region between both domains, labeled domain 1 and domain 2 in Fig. 4, is shown on an enlarged scale in the inset. The molecular rows within the different domains are oriented with an angle δ of about 14° in between. With respect to the $[11\bar{2}]$ direction the molecular rows are rotated by $+\delta/2$ and $-\delta/2$, respectively. At the domain boundary differently oriented and also disordered molecules are found (inset of Fig. 4). Furthermore the fuzzy appearance of some of the molecules at the domain boundaries can be interpreted as enhanced molecular diffusion there. The different line profiles across one molecular row in domains 1 and 2 are shown in Fig. 3(c) as upper and lower trace, respectively. The profiles were evaluated along the lines indicated by arrows in the inset of Fig. 4 and are perpendicularly averaged over 9 and 10 molecules. The upper trace in Fig. 3(c) corresponds to the upper domain in the inset of Fig. 4 and vice versa. Both line scans show internal structures as discussed before which are consistent with three higher and three lower maxima. The lower trace in Fig. 3(c) closely corresponds to the trace in Fig. 3(b), whereas the upper trace has the alternate sequence of higher and lower maxima. Note that both line scans in Fig. 3(c) closely match if the line scans are

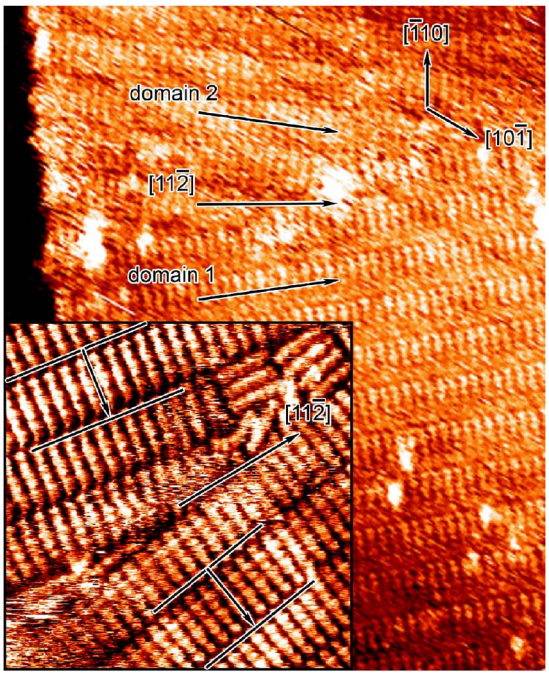

FIG. 4. (Color online) STM image of a α-sexithiophene monolayer on Au(111). Two nonequivalent domains are indicated (31×40 nm^2, −0.2 V, 0.5 nA). The inset displays the domain boundary on an enlarged scale (13×13 nm^2, −0.21 V, 0.3 nA).

mirrored at the center position of the 6T molecule. We therefore interpret the line profiles in Fig. 3(c) as fingerprints of left- and right-handed molecules. This observation proves that domains 1 and 2 in Fig. 4 are formed by molecules of opposite chirality.

To analyze the long-range order and to facilitate the interpretation of LEED data, the Fourier transform of the two-domain structure of Fig. 4 is shown in Fig. 5(a). In reciprocal space a complementary row structure is found which exhibits again the angle δ between the two domains as indicated in Fig. 5(a). Based on the oblique unit cell discussed above, the positions of possible LEED spots have been calculated. The right-hand side of Fig. 5(b) displays the expected diffraction (LEED) pattern for the two domain structures of Fig. 4 as open and filled circles, respectively. In general, the threefold symmetry of the Au(111) substrate results in three equivalent

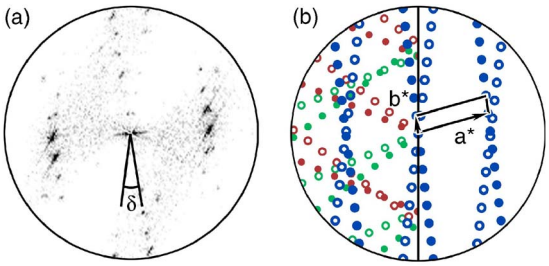

FIG. 5. (Color online) (a) Fourier transformation of the STM data of Fig. 4 and (b) calculated LEED pattern for two nonequivalent domains and for all six possible domains due to the threefold symmetry of the Au(111) substrate on the right-hand and left-hand sides, respectively.

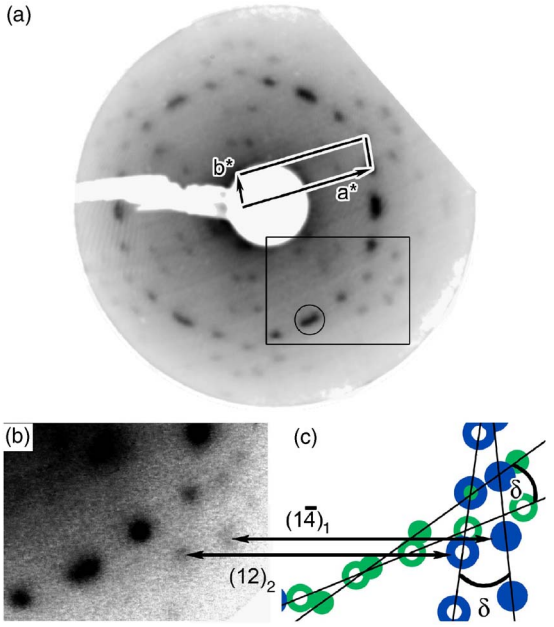

FIG. 6. (Color online) LEED pattern of a 6T monolayer on Au(111) at 20.0 eV (a). Enlargement of the lower right-hand section of the LEED pattern at 13.3 eV (b). Only four domains dominate in this section. (c) Calculated LEED pattern with four domains. The LEED spot order with respect to the reciprocal overlayer unit cell of the different rotational domains is indicated. The subscripts label the domains.

domains each. This leads to six different 6T domains in total which were all observed by STM (not shown here). The corresponding full reciprocal structure is sketched on the left-hand side of Fig. 5(b). Note that not all possible reciprocal spots will be present in the real LEED structure since several spots will have vanishing intensity due to the unit cell contents, namely the structure factor. The LEED pattern for the 6T monolayer on Au(111) at an electron energy of 20 eV is displayed in Fig. 6(a). Figure 6(b) shows an enlargement of the lower left-hand part of the LEED pattern for an electron energy of 13 eV together with the calculated reciprocal spot positions, Fig. 6(c). As expected not all possible spots are present in the LEED pattern which is dominated by the [10] and $[1\bar{1}]$ spots of the molecular superstructure. The $(0\ n)$ spots are generally weak and absent for certain electron energies. Such an energy (13 eV) has been chosen for the measurement of Fig. 6(b) so that mainly the $[1\ n]$ spots of four different domains are visible in the enlarged section of Fig. 6(b). The detailed analysis of the distances between different LEED spots allows determination of the unit cell parameters more accurately than the analysis of STM images. Especially the relative distance between adjacent spots of different domains as, e.g., the [1 2] spot of domain 2 and the $[1\bar{4}]$ spot of domain 1 as indicated in Figs. 6(b) and 6(c), allows high accuracy and reduces the influence of long range LEED screen distortions. This analysis of the 6T monolayer LEED data results in a unit cell which is described by a real space lattice vector **a** in row direction of 0.61 ±0.06 nm length oriented 7.0° ±0.5° off the $[11\bar{2}]$ direction. The second primitive unit cell vector **b**

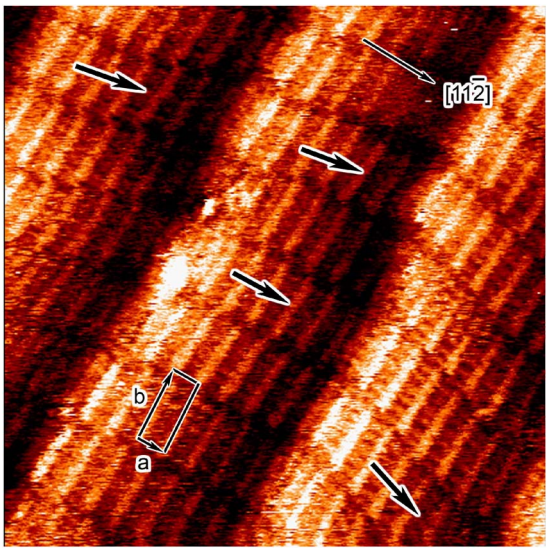

FIG. 7. (Color online) STM image of ordered molecules with enlarged unit cell found on narrower Au(111) terraces. The orientation of different stacks of 6T molecules are indicated by short arrows (20×20 nm^2, −0.19 V, 0.96 nA).

which is nearly perpendicular to the molecular rows has a length of 2.5 ±0.2 nm with an angle of 106.3° ±0.5° with respect to the $[11\bar{2}]$ direction. The deviation of the orientation vector **a**+**b** from 90° is small, but clearly visible in the separation of the [10] LEED spots of two mirrored domains. These spots are marked by a circle in Fig. 6(a) for domains 3 and 4. Also the vertical distance of the $[1\bar{2}]$ and the $[1\bar{4}]$ spots [marked in Fig. 6(b)] is only possible for an angle different from 90°. Note that the observed LEED structure is similar to the structure found for end-capped 6T on Ag(111) by Soukopp *et al.*[10] Besides the exact superstructure determination, the observed LEED pattern proves that the observed STM structures as discussed in Fig. 2 are the only dominant ones.

On highly stepped parts of the surface with narrow (111) terraces we also frequently found a different 6T structure. Figure 7 shows a 20×20 nm^2 STM image for such situation. On the narrow terraces shown, rows of only six and seven molecules are formed. The molecules align preferentially along the step edges as found similarly for larger terraces. However, on the narrower terraces the intrarow distance is strongly enlarged and also the shift between rows is now significantly less than one-half the intrarow distance. The resulting unit cell is indicated in Fig. 7. Compared to the dense monolayer unit cell, the unit cell vector **b** is approximately unchanged (2.4 nm), but the molecular intrarow distance is enlarged from 0.61 to about 1.0 nm. Alternatively, a structure with alternating upstanding and flat-lying molecules as found for the second layer of quaterrylene on Au(111) (Ref. 29) cannot be ruled out completely. Additionally the stacking of the molecules into rows shows some variations, mainly the sign of the row-to-row shift can change which leads to small angle rotation of the row direction. The different row orientations with respect to the $[11\bar{2}]$ direction are indicated by arrows in Fig. 7. Note that the

structures found on narrow terraces here are different from the structures reported for 6T adsorption on vicinal Au(111) surfaces by Mäkinen *et al.*[17] However, here the narrow-terrace structures are only a minority species which was not observed by LEED.

IV. DISCUSSION

The combination of STM and LEED reveals a dominant 6T monolayer structure with one molecule per unit cell forming six different long-range ordered domains. The detailed analysis of the LEED spots, especially between adjacent spots of different domains, leads to an incommensurate structure which can be approximately described in matrix notation with respect to the unreconstructed Au(111) substrate by

$$\begin{pmatrix} 2.4 & 1.5 \\ -2.8 & 6.8 \end{pmatrix}$$

and its mirror image. Note that we follow the convention of Barlow and Raval for the choice of unit cell vectors.[23] The periodic structure corresponds to a dense molecular packing with 0.67 molecules/nm^2. This structure is planar and different from any bulk lattice plane of a 6T single crystal.[4,5] Although in 6T single crystals all molecules are strongly planar and in all-*trans* conformation, there are two molecules per unit cell which are tilted against each other to form a herringbone packing common to many planar organic molecules.[5] The structure reported in our work is of about 20% higher density as compared to a monolayer of end-capped 6T on Ag(111) where an adsorbate density of 0.52 molecules/nm^2 has been reported.[10] However, this might be well induced by the large end-groups of end-capped 6T which affect the lattice structure. To our knowledge, there are no monolayer unit cell data for 6T adsorption on any other flat metal surfaces available for comparison. The important question of what drives the molecular structure within the monolayer needs to be discussed further: The intermolecular forces (e.g., the van der Waals attraction and the Pauli repulsion) determine the bulk 6T crystal structure and are expected to determine the structure of thin molecular films, too. However, the first monolayer on metallic as well as on dielectric substrates is strongly influenced by the molecule-substrate interaction which might be physisorption or weak π interaction. For large planar organic molecules on close-packed metal substrates, as on Au(111), this often results in monolayers of flat-lying coplanar molecules—structures which are absent in the respective bulk crystals. Additionally the monolayer-substrate interaction results in a well-defined orientation of long-range ordered domains as will be discussed below. In our case the monolayer-substrate interaction seems to be only weakly site-specific based on the observed incommensurability of the monolayer.

In the following we demonstrate that many aspects of the monolayer structure can be widely explained by the intermolecular interactions in the monolayer and the two-dimensional shape (van der Waals contour) of the flat-lying molecules. The resulting structure will be different from any plane of a 6T single crystal, mainly because the molecule-substrate interaction strongly favors completely coplanar structures. For the discussion we assume a rather rigid all-trans molecular structure as is found experimentally by high-resolution STM images [see Fig. 2(e)] with a fixed shape of the molecules as sketched in Fig. 1(c). Possible two-dimensional (2D) close-packing structures are illustrated in Figs. 8(a), 8(d), and 8(e), for rows of homochiral molecules. The parallel stacking of the molecules into rows optimizes the close packing as well as the van der Waals attraction between the molecules as depicted in Fig. 8(a). The two rectangular regions outlined in Fig. 8(a) are enlarged in Figs. 8(b) and 8(c). Figure 8(c) shows how the different sides of the thiophene rings of adjacent molecules can gear into each other. At this point an equivalent close packing between two molecules of different chirality could be also possible. However, this would imply that both molecules are shifted by one thiophene ring with respect to each other. Since this would decrease the length of contact (number of thiophene rings) and would also decrease the packing density, it is less favored unless another mechanism, e.g., a strong molecule-substrate interaction, gains energy by such a molecular shift.

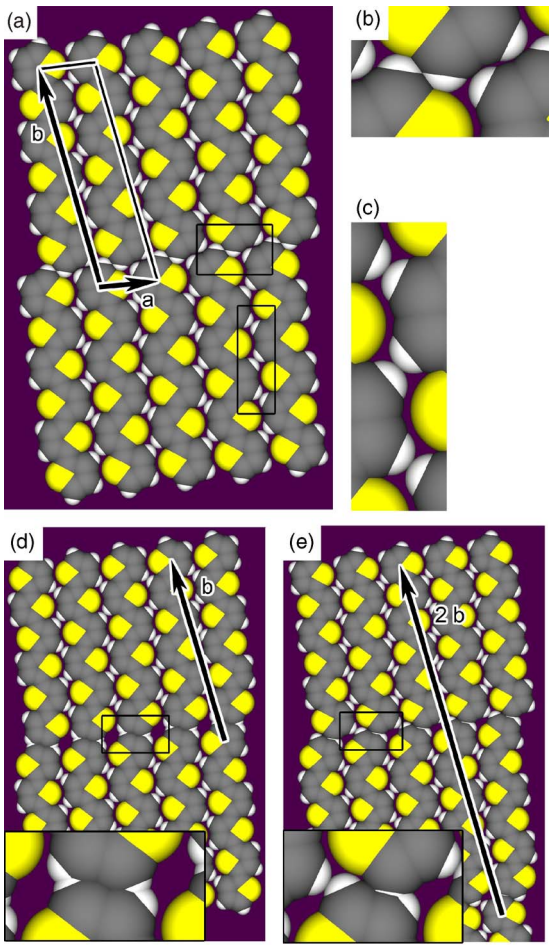

FIG. 8. (Color online) Schematic model of the arrangement within a 6T monolayer: Structure of a homochiral domain (a); the marked rectangular areas are enlarged in (b) and (c). Structure for a homochiral domain of opposite chirality (d) and for rows of alternating chirality (e). The insets show enlargements of the marked areas.

We hypothesize that the optimization of the contact length between neighboring molecules defines largely the structure as this is related to the configuration with the highest total van der Waals attraction. Therefore the attraction between two molecules leads to a chiral homorecognition. The same argument of close packing holds for the interaction between adjacent molecular rows as is illustrated in the enlargement in Fig. 8(b) for the case of rows of homochiral molecules. The attractive interaction between adjacent rows is optimized by a small translation in row direction for adjacent rows. It allows that the ends of the molecules of one row slide into the space between the molecules of the adjacent row. Note that the model shown in Fig. 8 is based on the experimentally determined dimensions of the monolayer unit cell. It can be seen that the contact between adjacent homochiral rows is optimized by this procedure which nicely explains the experimentally found row-to-row distance, shift, and the resulting nonrectangular unit cell. As can be seen from the details in Figs. 8(b) and 8(c), the asymmetric structure of the thiophene ring allows a rather compact structure also between the molecular rows. This discussion illustrates that the experimentally found homochirality within a single domain can be understood as chiral homorecognition during growth of the monolayer.

The close packing within a *homochiral* domain of identical unit cell but with molecules of *opposite* chirality as compared to Fig. 8(a) is illustrated in Fig. 8(d). Whereas the intrarow interactions are unchanged, the interrow interaction strongly unfavors this structure. This is seen best in the enlarged inset in Fig. 8(d). The comparison of the structures shown in Figs. 8(a) and 8(d) demonstrates that the specific form of the unit cell defines the specific chirality of the molecules in this domain and vice versa. All molecules with opposite chirality will arrange only in the structure with mirrored unit cell as found experimentally and discussed in Figs. 4 and 3(c). Such a coupling of the specific point and organizational chirality has been observed also for other adsorption systems.[30]

Finally, the situation for molecular rows with *alternating* row-to-row chirality is illustrated in Fig. 8(e). Again the badly matching contours—as is seen in the inset of Fig. 8(e)—in comparison to the favored situation shown in Fig. 8(b) rules out such a structure of heterochiral molecules. Experimentally the identical line profiles discussed in Fig. 3(b) rule out this structure. Note that the situation shown in Fig. 8(e) corresponds to a doubled unit cell with two molecules. However, the corresponding additional half-order superstructure LEED spots were not observed experimentally.

In summary, the consequently close-packed arrangement for the given unit cell structure nicely explains the occurrence of large homochiral domains and the absence of heterochiral structures. The mirror (and symmetry nonequivalent) domain corresponds to the arrangement of molecules of the opposite chirality as observed by STM and LEED. Its structure is equivalent to the mirror plane image with respect to the $[11\bar{2}]$ high-symmetry direction.

Note that the 6T molecule is prochiral in the gas phase and only upon adsorption the flat-lying molecules separate into equal fractions of right-handed and left-handed species.

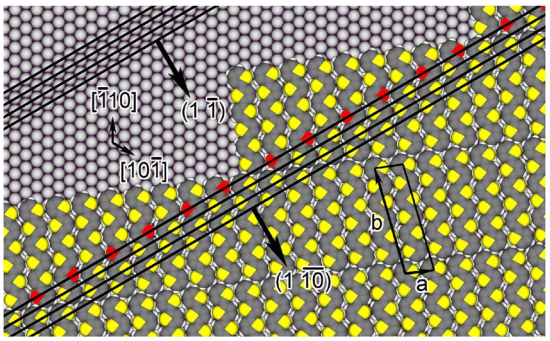

FIG. 9. (Color online) Schematic model of the 6T monolayer. The line-on-line arrangement of the Au first layer $(1\bar{1})$ and the 6T $(1\bar{1}0)$ Bragg planes are emphasized by solid lines. The latter is a adlayer reciprocal lattice point for which all sulfur atoms contribute in phase.

Initial adsorption leads to a racemic mixture and the surface possesses no overall chirality. The chiral separation into larger domains requires therefore the transport of molecules. This might explain that on narrow terraces where transport is quasi-one-dimensional as in Fig. 7, the separation is more difficult and structures of molecules with different chirality are found.

Based on the assumptions of close packing and the specific shape of the molecule, the details of the monolayer structure and its chiral separation can be rationalized. However, the molecule-substrate interaction must be responsible for the orientation of the incommensurate monolayer with respect to the substrate: Here a well-defined angle of +7° or −7° between the molecular rows and the $[11\bar{2}]$ direction is experimentally observed depending on the chirality of the molecular domains. This implies that neither the primitive unit cell vectors nor the orientation of the molecules are aligned with any Au(111) high-symmetry direction. In the following we show that the orientation can be understood based on a line-on-line monolayer growth on Au(111). As has been discussed previously, the point-on-line and the line-on-line alignments allow for incommensurate structures in real space which are however "commensurate" or "higher-order commensurate" in reciprocal space, respectively.[31] The coinciding Fourier components of the interaction potential can define a local minimum in the potential energy, although the structure needs not to be commensurate in real space. For the 6T monolayer on Au(111), the $(1,\bar{1}0)$ and the $(1,\bar{1})$ reciprocal lattice points (Bragg planes) of the organic adlayer and the substrate, respectively, coincide. This is illustrated in Fig. 9 which shows the orientation of the organic monolayer with respect to the Au(111) substrate. In the upper left-hand part of Fig. 9 the substrate $(1,\bar{1}0)$ lattice planes are indicated by solid lines. For the organic layer the $(1,\bar{1}0)$ lattice planes with respect to the 6T unit cell are shown as solid lines. Both sets of parallel lines in Fig. 9 illustrate that the Au $(1,\bar{1})$ and the 6T $(1,\bar{1}0)$ Bragg planes coincide. This coincidence is the reason for the rotational orientation of the organic layer. Since the orientation determination is based on LEED data and since no atomic resolution of the Au(111) substrate has

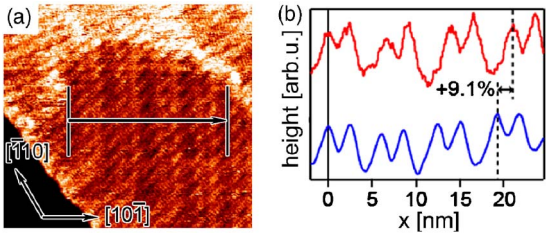

FIG. 10. (Color online) (a) STM image of an 6T monolayer on Au(111) (45×40 nm^2, −0.2 V, 0.65 nA). (b) Line profile across the herringbone reconstruction in the presence of the 6T monolayer (upper trace) and for the bare Au(111) surface (lower trace). The line profile is indicated in (a) and averages perpendicular to the profile direction as indicated by bars.

been achieved in the presence of rows of molecules, the position of the adlayer with respect to a *rigid shift* in the substrate $[11\bar{2}]$ direction is not defined yet.

Although it is speculative to explain the experimentally found orientation of the monolayer without detailed calculations of the molecule-substrate interactions, we point out that the positions of *all* sulfur atoms are located on the $(1,\bar{1}0)$ lattice planes. This is clearly visible in Fig. 9 where all sulfur atoms which fall on one $(1,\bar{1}0)$ lattice line are indicated. It can be seen that the alignment of the sulfur atoms proceeds perfectly from row to row. The physical origin of the underlying interaction might be a rather local sulfur-Au(111) interaction or, more likely, the specific interaction of the 6T valence π-orbitals with the gold layer underneath. The valence π-orbitals with quinoid character have an enhanced p_z-like electron density at the sulfur sites[32] and might be the origin for the remaining site specificity. Further support for such a molecular site-specific substrate interaction comes from a related system: For end-capped quarterthiophene on Ag(111) a stretching of the internal C-S bonds together with a small distortion of the thiophene rings has been found by surface x-ray diffraction.[13,33] In this commensurate adsorption system the positions of the thiophene S atoms are close to on top.[13] For the incommensurate 6T monolayer on Au(111) one might expect therefore S positions along the close-packed Au rows, shifting between on-top and bridge positions.

An additional aspect which needs further discussion is the herringbone reconstruction of the top metal layer which is still present upon 6T monolayer adsorption as has been seen in Figs. 2(c) and 10(a). On the bare Au(111) surface shown in Figs. 2(a) and 2(b), surface stress leads to the well-known $(22\times\sqrt{3})$ superstructure with a compression in the top layer of 4.4%.[26,27] The reconstruction of the bare surface can be described by a stacking-fault-domain model involving periodic transitions from fcc to hcp stacking of the top-layer Au atoms.[28] This leads to a practically uniform contraction in the surface layer which relaxes the intrinsic tensile stress by 22%.[34] Adsorption of a 6T monolayer will modify the Au(111) electronic structure and will alter the surface stress accordingly. In fact we observe that the long-range herringbone reconstruction is preserved upon 6T adsorption but with slightly modified periodicity. STM images on large 6T monolayer domains as in Fig. 10(a) indicate that the distance between the soliton-type domain walls is enlarged upon 6T monolayer adsorption. The lower and the upper trace in Fig. 10(b) show the line profiles across the herringbone reconstruction for the bare and the 6T covered Au(111) surface [averaged perpendicularly as indicated in Fig. 10(a)]. The positions of the domain walls are clearly visible as maxima in the line profiles. The superstructure periodicity is changed from a width of 22 Au-Au next-neighbor distances for the clean surface to about 24 lattice constants upon 6T adsorption at room temperature. This corresponds to a reduction of the top most Au layer compression from 4.4% for the bare Au surface to 4.2% upon 6T adsorption. Indications of similar modifications of the Au(111) herringbone reconstruction have been reported earlier for C_{60}, hexa-perihexabenzocoronene (HBC), and perylenetetracarboxylic-dianhydrid (PTCDA) adsorption.[35–37] Note that on Au(111) upon 6T adsorption the different lengths of the straight reconstruction segments between 120° rotations [as seen in Figs. 2(c) and 10(a)] might reflect the slightly asymmetric strain due to the locking with respect to the line-on-line registry.

V. SUMMARY

Based on LEED and STM measurements the monolayer structure of α-sexithiophene on Au(111) has been determined: Thermally sublimated 6T molecules adsorb in a flat-lying geometry with all-*trans* conformation of the thiophene rings. Upon adsorption at 300 K, they are separated into right- and left-handed molecules. Large homochiral domains of both handiness' are found. The observed chiral separation within the monolayer might be used as a template for subsequent enantiomeric selective growth of thin films. The monolayer structure with one molecule per unit cell consists of molecular rows oriented +7° (or −7°) off the three equivalent $[11\bar{2}]$ high-symmetry directions. The domains are incommensurate with respect to the Au(111) substrate. The unit cell structure and the chiral homorecognition during domain growth can be rationalized based on the shape of the 6T molecule and the molecule-molecule interactions within the adlayer. A line-on-line arrangement where the $(1,\bar{1})$ Bragg planes of the first layer Au atoms coincide with the $(1,\bar{1}0)$ Bragg planes of the molecular monolayer, defines the orientation of the domains. Additionally the Au(111) herringbone reconstruction is relaxed upon 6T adsorption to a first Au layer compression of 4.2%.

ACKNOWLEDGMENTS

The authors thank Ralf Kulla for technical support. Financial support by the Deutsche Forschungsgemeinschaft through Contract No. SFB 418 is gratefully acknowledged.

[1] E. Umbach, M. Sokolowski, and R. Fink, Appl. Phys. A: Mater. Sci. Process. **63**, 565 (1996).
[2] G. Witte and C. Wöll, J. Mater. Res. **19**, 1889 (2004).
[3] P. Leclere, M. Surin, P. Viville, R. Lazzaroni, A. F. M. Kilbinger, O. Henze, W. J. Feast, M. Cavallini, F. Biscarini, A. P. H. J. Schenning, and E. W. Meijer, Chem. Mater. **16**, 4452 (2004).
[4] D. Fichou, J. Mater. Chem. **10**, 571 (2000).
[5] G. Horowitz, B. Bachet, A. Yassar, P. Lang, F. Demanze, J. L. Fave, and F. Garnier, Chem. Mater. **7**, 1337 (1995).
[6] A. Soukopp, C. Seidel, R. Li, M. Bässler, M. Sokolowski, and E. Umbach, Thin Solid Films **285**, 343 (1996).
[7] M. B. Nardelli, D. Cvetko, V. DeRenzi, L. Floreano, R. Gotter, A. Morgante, M. Peloi, F. Tommasini, R. Danieli, S. Rossini, C. Taliani, and R. Zamboni, Phys. Rev. B **53**, 1095 (1996).
[8] T. Okajima, S. Tanimura, K. Hamano, T. Kurata, Y. Uehara, T. Ogama, H. Koezuka, S. Narioka, T. Araki, and Y. Ouchi, J. Electron Spectrosc. Relat. Phenom. **78**, 379 (1996).
[9] W. Gebauer, C. Väterlein, A. Soukopp, M. Sokolowski, R. Hock, H. Port, P. Bäuerle, and E. Umbach, Synth. Met. **87**, 127 (1997).
[10] A. Soukopp, K. Glockler, P. Kraft, S. Schmitt, M. Sokolowski, E. Umbach, E. Mena-Osteritz, P. Bäuerle, and E. Hadicke, Phys. Rev. B **58**, 13882 (1998).
[11] S. Prato, L. Floreano, D. Cvetko, V. De Renzi, A. Morgante, S. Modesti, F. Biscarini, R. Zamboni, and C. Taliani, J. Phys. Chem. B **103**, 7788 (1999).
[12] M. Rei Vilar, G. Horowitz, P. Lang, O. Pellegrino, and A. M. Botelho do Rego, Adv. Mater. Opt. Electron. **9**, 211 (1999).
[13] L. Kilian, W. Weigand, E. Umbach, A. Langner, M. Sokolowski, H. L. Meyerheim, H. Maltor, B. C. C. Cowie, T. Lee, and P. Bäuerle, Phys. Rev. B **66**, 075412 (2002).
[14] M. Kiguchi, S. Entani, K. Saiki, and G. Yoshikawa, Appl. Phys. Lett. **84**, 3444 (2004).
[15] M. Kiguchi, G. Yoshikawa, S. Ikeda, and K. Saiki, Surf. Sci. **566**, 603 (2004).
[16] G. Yoshikawa, M. Kiguchi, S. Ikeda, and K. Saiki, Surf. Sci. **559**, 77 (2004).
[17] A. J. Mäkinen, J. P. Long, N. J. Watkins, and Z. H. Kafafi, J. Phys. Chem. B **109**, 5790 (2005).
[18] C. E. Heiner, J. Dreyer, I. V. Hertel, N. Koch, H.-H. Ritze, W. Widdra, and B. Winter, Appl. Phys. Lett. **87**, 093501 (2005).
[19] H. Inoue, G. Yoshikawa, and K. Saiki, Jpn. J. Appl. Phys., Part 1 **45**, 1794 (2006).
[20] J. Ivanco, T. Haber, R. Resel, F. P. Netzer, and M. G. Ramsey, Thin Solid Films **514**, 156 (2006).
[21] M. Kiguchi, G. Yoshikawa, and K. Saiki, J. Appl. Phys. **94**, 4866 (2003).
[22] T. Haber, S. Muellegger, A. Winkler, and R. Resel, Phys. Rev. B **74**, 045419 (2006).
[23] S. M. Barlow and R. Raval, Surf. Sci. Rep. **50**, 201 (2003).
[24] F. Balzer and H. G. Rubahn, Appl. Phys. Lett. **79**, 3860 (2001).
[25] M. A. Van Hove, R. J. Koestner, P. C. Stair, J. P. Biberian, L. L. Kesmodel, I. Bartos, and G. A. Somorjai, Surf. Sci. **103**, 189 (1981).
[26] U. Harten, A. M. Lahee, J. P. Toennies, and C. Wöll, Phys. Rev. Lett. **54**, 2619 (1985).
[27] C. Wöll, S. Chiang, R. J. Wilson, and P. H. Lippel, Phys. Rev. B **39**, 7988 (1989).
[28] J. V. Barth, H. Brune, G. Ertl, and R. J. Behm, Phys. Rev. B **42**, 9307 (1990).
[29] R. Franke, S. Franke, C. Wagner, T. Dienel, T. Fritz, and S. C. B. Mannsfeld, Appl. Phys. Lett. **88**, 161907 (2006).
[30] M. Schöck, R. Otero, S. Stojkovic, F. Hummelink, A. Gourdon, E. Laegsgaard, I. Stensgaard, C. Joachim, and F. Besenbacher, J. Phys. Chem. B **110**, 12835 (2006).
[31] S. C. B. Mannsfeld, K. Leo, and T. Fritz, Phys. Rev. Lett. **94**, 056104 (2005).
[32] C. Ziegler and D. Fichou, *Handbook of Oligo-and Polythiophenes* (Wiley-VCH, New York, 1999).
[33] H. L. Meyerheim, T. Gloege, H. Maltor, M. Sokolowski, E. Umbach, and P. Bäuerle, Surf. Rev. Lett. **6**, 883 (1999).
[34] C. E. Bach, M. Giesen, H. Ibach, and T. L. Einstein, Phys. Rev. Lett. **78**, 4225 (1997).
[35] J. K. Gimzewski, S. Modesti, C. Gerber, and R. R. Schlittler, Chem. Phys. Lett. **213**, 401 (1993).
[36] F. Sellam, T. Schmitz-Hübsch, M. Toerker, S. Mannsfeld, H. Proehl, T. Fritz, K. Leo, C. Simpson, and K. Müllen, Surf. Sci. **478**, 113 (2001).
[37] L. Kilian, E. Umbach, and M. Sokolowski, Surf. Sci. **600**, 2633 (2006).